Shahid Chamran University of Ahvaz

Irrigation Sciences and Engineering (JISE)
Vol. 44, No. 2, Summer 2021, p. 25-38

Original Paper

Journal homepage: https://jise.scu.ac.ir

Investigation of the Effect of Ramp Angle on Chute Aeration System Efficiency by Two-Phase Flow Analysis

B. Lashkar-Ara[1*] and L. Najafi[2]

1- Corresponding Author, Associate Professor, Civil Engineering Department, Jundi-Shapur University of Technology, Dezful, Iran (Lashkarara@jsu.ac.ir).*
2- Instructor in Civil Engineering Department Jundi-Shapur University of Technology, Dezful,Iran..

ARTICLE INFO

Artlcle history:
Received: 26 May 2021
Revised: 17 July 2021
Accepted: 18 July 2021

Keywords:
Aeration system, Ramp angle, Aeration coefficient, Two-phase flow, Flow-3D model.

TO CITE THIS ARTICLE:

Lashkar-Ara, B., Najafi, L. (2021). 'Investigation of the Effect of Ramp Angle on Chute Aeration System Efficiency by Two-Phase Flow Analysis', Irrigation Sciences and Engineering, 44(2), pp. 25-38. doi: 10.22055/jise.2021.37743.1980.

Abstract

Flow aeration in chute spillway is one of the most effective and economic ways to prevent cavitation damage. Surface damage is significantly reduced when very small values of air are scattered in a water prism. A structure known as an aerator may be used for this purpose. Besides, ramp angle is one of the factors influencing aerator efficiency. In this research, the value of air entraining the flow through the Jarreh Dam's spillway at the ramp angles of 6, 8 and 10 degrees, as three different scenarios, was simulated using the Flow-3D software. In order to validate the results of the inlet air into the flowing fluid at a ramp angle of 6 degrees, the observational results of the dam spillway physical model from the laboratory of TAMAB Company in Iran were used. According to the results, raising the ramp angle increases the inlet air to the water jet nappe, and a ten-degree ramp angle provides the best aeration efficiency. The Flow-3D model can also simulate the two-phase water-air flow on spillways, according to the results.

Introduction

Aerators are used to prevent cavitation in chute spillways. According to the literature, the entrained air through the free surface of the flow may protect the spillway floor from cavitation damage if the free-surface aeration process provides a sufficient air concentration near the bottom (i.e. C>7%) (Chanson, 1989). Many researchers have used computational fluid dynamics to simulate complex flow problems in most hydraulic structures (Baharvand and Lashkar-Ara, 2021; Dong et al. 2019; Mahmoudian et al. 2019).

Wang et al. (2012) examined an aerator in stepped chute of a hydraulic power station to look into cavitation damage. Based on the results, the aerator effectively prevents cavitation. Xu et al. (2012) conducted a hydrodynamic and momentum analysis on an aerator to prevent cavitation damage. They proposed a relation to estimate the depth of backwater in the aerator. Wu et al. (2016) tested out a new ski-jump-step spillway with an aeration basin. Physical experiments revealed that this form of spillway was more efficient than traditional stepped spillways in the prevention of energy loss and cavitation. Zhang and Chanson (2016) conducted experiments to test how free-surface aeration and total pressure affect the stepped chute spillway. According to the results, these types of spillways have a significant effect on energy dissipation. Wei et al. (2016)

investigated the self-aeration procedure in supercritical chute spillway. They obtained an empirical equation to predict the self-aeration procedure. Kherbache et al. (2017) used the Reynolds averaged Navier-Stokes equation (RANS) and volume of fluid (VOF) to numerically simulate air-water flow over stepped spillway. The results showed that air injection increases the pressure on steps. Bayon et al. (2018) investigated the mechanism of non-aerated regions in stepped spillways and the starting point of aeration in this type of spillways to understand the aerator's behavior in self-aerated regions. They used OpenFOAM, FLOW-3D®, Partial VOF (Volume of Fluid) and "True" VOF (TruVOF) to perform numerical modeling. In this type of spillway, they derived results from flow velocity, turbulent kinetic energy, and tangential stress. Parsaie and Haghiabi (2019) investigated the location of the starting point of aeration in quarter-circular crested stepped spillways (QCSS) using experiments and dimensional analysis. According to their results, the distance between the inception point of flow aeration and the crest increases as the flow rate increases. Yang et al. (2019) studied the two-phase flow in chute spillway aerators using computational fluid dynamics (CFD). The results showed that the aerator layouts have a significant impact on the water-air flow. Kramer and Chanson (2019) used a physical model and ran a sensitivity analysis on highly aerated flows in stepped spillways. They demonstrated that flow velocity in void regions could be improved. Numerical methods, such as computational fluid dynamics, have advanced rapidly in recent years as a result of developments in hydroinformatics, which requires less time and cost to study flow conditions than physical models. Since the hydraulic conditions of the flow passing through the spillway structure were evaluated prior to the construction of the structure, the researchers had a positive view on the hydraulic conditions of the flow passing through the structure. This method can be used to design structures and control the corrosion phenomenon.

In this study, using the Flow-3D model, the efficiency and effect of the spillway aeration ramp angle of the Jarreh Dam were investigated under various flow conditions. The results of the laboratory research conducted at the Water Research Institute (TAMAB in Persian) on the physical model of the Jarreh Dam's spillway were used to validate the model. For this purpose, after measuring the average concentration of air in the aeration area, the value of air entraining the flow jet was calculated for three angles of 6, 8, and 10 degrees (before the collision region). Besides, this study can evaluate the ability of the Flow-3D model to analyze the mixture of air and water in the two-phase flow in chute spillways.

Aeration Mechanism

In aerators, a deflector separates the flow from the bed, resulting in a free jet. Air entrains the jet from above and below due to turbulence. Air entrainment, especially from the bottom surface of the jet, increases the air concentration near the concrete surface. The most common types of aerators are shown in Fig. (1). As shown in this figure, air is supplied for the surface below the fountain through a duct from the floor, ensuring that the flow is fully aerated and that cavitation damage is avoided due to the air near the spillway floor. In order to understand how aeration works, the flow near the aerator is usually divided into a number of regions. For example, in Fig. (1), the flow near the aerator is divided into the following 5 regions (Chanson, 1989).

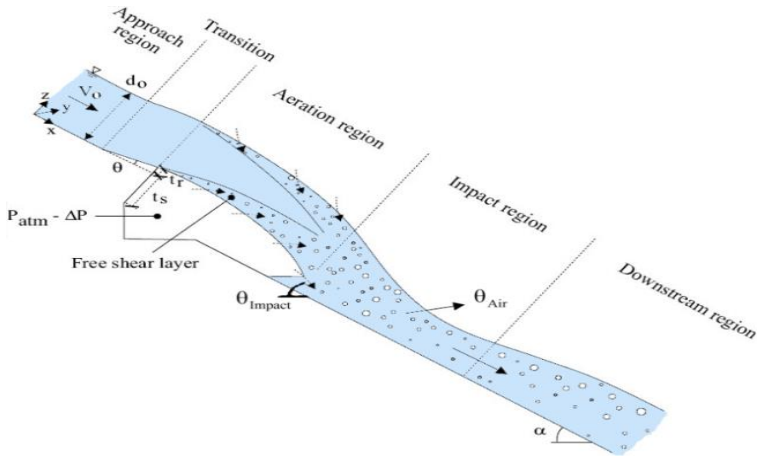

Fig. 1- Schematic of the general pattern of flow and aeration process in the aerators

Approach region characteristics such as velocity, intensity of turbulence and the value of air in the water affect the flow behavior in the aerator. In order for air to entrain water from the flow surface, it is necessary for the turbulent boundary layer to reach the water surface (natural aeration), and subsequently there must be enough space for the air to mix and reach the lower layers of the flow.

The transition region corresponds to the length of the deflector. At the beginning of the deflector, the pressure on the bed becomes more than the hydrostatic pressure; however, as soon as the jet starts, the pressure will be equal to the pressure below the jet, i.e. negative. In general, the flow depth changes along the deflector, the boundary layer becomes thinner, the shear stress on the spillway floor increases, and the value of turbulence increases. The aeration region starts from where the flow leaves the deflector. Turbulence disperses air within the jet as air approaches from the bottom and top layers of the water jet nappe. The water and air layers formed above and below the jet gradually develop as the jet moves downstream. If the length of the downstream jet movement is long enough, these layers reach together, and the jet nappe is completely aerated (Chanson, 1989).

In the Impact region, the pressure gradient is greater than the hydrostatic pressure. Owing to the rapid changes in air distribution induced by large pressure gradients, the distribution of air concentration will also change significantly. At the beginning of the downstream region is the collision region, where the pressures are higher than the hydrostatic pressures and the movement of air bubbles to the water surface is intense. After a distance, pressure returns to being hydrostatic.

Materials and Methods

Experimental Setup

For simulation, the laboratory model of Jarreh Dam, which was built at a scale of 1:50 in the laboratory of Iran Water Resources Research Center, was used. It should be noted that the overflow of Jarreh dam is practically devoid of aeration, but in research conducted in parallel with the final model of this overflow by Shamloo et al. (2012), the issue of aerator location and its effect on flow aeration were studied. The simulation results were compared using the results of Shamloo et al. (2012).

Jarreh Reservoir Dam, on the Zard River, one of the major tributaries of the Jarahi River, is 35 kilometers northeast of Ramhormoz city and has a gated chute spillway and an emergency spillway. The main gated spillway includes approach channel, gated weir, chute and flip bucket. Fig (2) shows a view of the physical modeling of Jarreh Dam in TAMAB laboratory.

Governing Equations

The 3D Reynolds-averaged Navier–Stokes (RANS) equations for one fluid were numerically solved using the commercial CFD code FLOW-3D® (Flow-3D, 2017), which included the RNG k- turbulence model (Yakhot & Orszag, 1986) and the TurVOF method (Hirt & Nichols, 1981) to track the interface. The current study did not take into

 DOI: 10.22055/JISE.2021.37743.1980

account sediment transport or cavitation processes.

Mass Continuity Equation

The continuity equation for incompressible two-phase flow is expressed by the volume-weighted average density and velocity of two phases as follows:

$$\frac{\partial \rho_m}{\partial t} + \nabla \times (\rho_m u_m) - \nabla \times (\vartheta \nabla \rho_m) = 0 \qquad (1)$$

where u_m and ρ_m are the velocity and volume-weighted average density, respectively. The third term on the left-hand side signifies turbulent diffusion, which seems to be logical only for turbulence mixing processes for fluids with non-uniform densities. ϑ equals $S_c \mu_m / \rho_m$, where μ_m is the volume-weighted average dynamic viscosity and S_c is a constant that is equal to the reciprocal of the turbulent Schmidt number.

Momentum Equation

The following equation describes the momentum conservation of a fluid mixture:

$$\frac{\partial (\rho_m u_m)}{\partial t} + \nabla \times (\rho_m u_m u_m) = -\nabla P + \rho_m g + \nabla \times \tau \qquad (2)$$

where **g** is the gravitational acceleration, P is pressure, and τ is the Reynolds stress tensor. The Boussinesq hypothesis is used to calculate τ via the effective kinematic viscosity, ϑ_{eff}, the turbulent kinetic energy, k, and the identity matrix, **I**:

$$\tau = -\vartheta_{eff} \left(\nabla u_m + \nabla u_m^T - \frac{2}{3} I \nabla u_m \right) + \frac{2}{3} Ik \qquad (3)$$

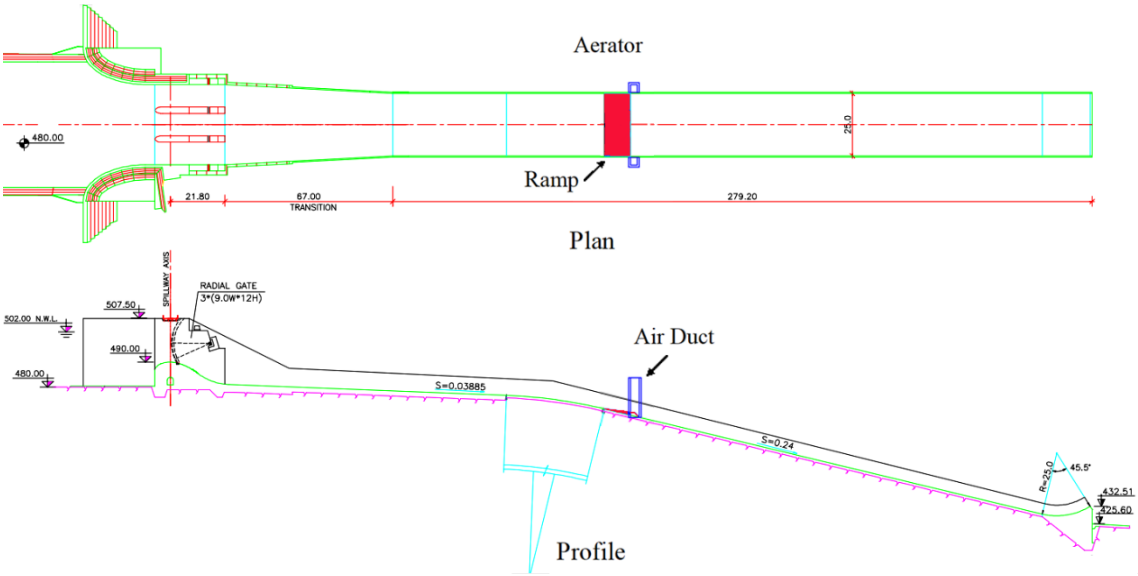

(a) The full-scale map of the Jarreh spillway's plan and profile.

(b) The physical model at a scale of 1:50

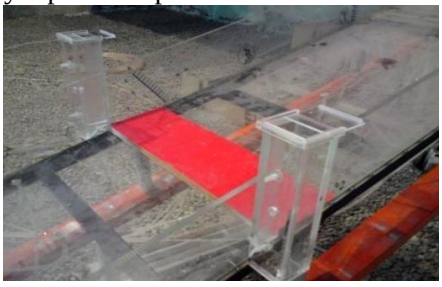

(c) Aerator device

Fig. 2- Experimental setup (Shamloo et al., 2012)

RNG k-ε Turbulence Model

The RNG k-ε model was used to model turbulence considering the impact of finer motion scales for the flow including strong shear and complex geometries. The following equations are the governing equations of the turbulence model:

$$\frac{D}{Dt}(\rho_m k) = \nabla \times (\rho_m D_k \nabla k) + P_k - \rho_m \varepsilon \quad (4)$$

$$\frac{D}{Dt}(\rho_m \varepsilon) = \nabla \times (\rho_m D_\varepsilon \nabla_\varepsilon) + \frac{C_1 P_k \varepsilon}{k} - \frac{C_2^* \rho_m \varepsilon^2}{k} \quad (5)$$

where D_k and D_ε are the effective diffusivity of k and ε, and P_k is the k generation by the mean velocity gradients. The model parameter C_1 is 1.42, and C_2^* can be computed by C_2 = 1.68, P_k, and k. The software's user manual (Flow-3D, 2017) presents more information about the RNG k-turbulence model.

VOF Model

TruVOF method is used for Flow-3D and traces the interface of two immiscible fluids through an indicator scalar, from 0.0 to 1.0, to present the fractional volume for water (as the main fluid in this research) for all the computational cells. Moreover, to apply the boundary conditions in the interface, TruVOF is used, which removes the need to calculate the equations in the air phase and remarkably speed up the simulation. The following equation is transport equation for *f*:

$$\frac{\partial f}{\partial t} + u_m \nabla f - \nabla \times (\vartheta \nabla f) = 0 \quad (6)$$

As in Equation (1), the third left-side term refers to turbulent diffusion.

Air Entrainment Model

In FLOW-3D® model, it is assumed that air entrainment is obtained when turbulence-induced instabilities defeat the stabilizing forces, P_d, arising from surface tension and gravity (Hirt, 2003; Meireles et al., 2014). Eq. (8) represents the P_d force. It should be noted that when instabilities owing to turbulence develop at the free surface, air entrainment occurs. The following governing equations explain air volume entered into the fluid:

$$L_T = \frac{\mathrm{CNU}^{3/4} k^{3/2}}{\varepsilon_T} \quad (7)$$

$$P_t = \rho_\omega k \;\; ; \;\; P_d = \rho_w g_n L_T + \frac{\sigma_{sur}}{L_T} \quad (8)$$

$$\delta V = \begin{cases} k_{air} A_s \left[\frac{2(P_t - P_d)}{\rho_w} \right]^{1/2} & if \quad P_t > P_d \\ 0 & if \quad P_t > P_d \end{cases} \quad (9)$$

where L_T is the turbulence length scale, CNU is a constant and equal to 0.09, and k_T and ε_T are the turbulent kinetic energy and turbulent dissipation, respectively. The ρ_w is the water density, g_n is the gravity component normal to the water surface, σ_{sur} is the surface tension coefficient, δV is the air entrained volume per unit time, k_{air} is a proportionality coefficient, and A_s is the surface area. The air entrainment is integrated with a single-phase fluid mixture model in FLOW-3D®, where air is supplied to the fluid as a passive tracer without altering the fluid flow directly (for example, lack of momentum transfer and lack of voids caused by bubbles), yet changing the fluid density based on the air concentration. When the entrained air concentration into the computational cells is smaller than 10%, this method is trustworthy (Hirt, 2003). Additional physical processes of air transport in the water are evaluated using Bulking and buoyancy factors. The drift-flux models and density evaluation described below can be used to implement these.

Density Evaluation Model

The density evaluation model seeks to compute the entrained air's non-uniform fluid density; therefore, the mixture density can be calculated as follows:

$$\rho_m = (1 - C_a)\rho_w + C_a \rho_a \quad (10)$$

where ρ_a and ρ_m are the air density and mixture density, respectively, and C_a shows the air concentration.

 DOI: 10.22055/JISE.2021.37743.1980

Drift-Flux Model

The drift-flux model can simulate phase drag, buoyancy, and bubble particle interaction (Brethour & Hirt, 2009). The relative velocity among dispersed air bubbles and continuous water is assumed to remain constant in the model, and hence the air transport equation is expressed as follows:

$$\left(\frac{1}{\rho_w}-\frac{1}{\rho_a}\right)\nabla P=\left(\frac{f\rho_w+(1-f)\rho_a}{f(1-f)\rho_w\rho_a}\right)K u_r \quad (11)$$

f is the water volume fraction, K is the cell drag coefficient, and u_r shows the relative/slip velocity in Equation (5). The single particle drag coefficient, K_p, can be used to compute K:

$$K_p=\frac{1}{2}A_p\rho_\omega\left(C_d U_r+\frac{12\mu_w}{\rho_w R_p}\right) \quad (12)$$

$$K=\frac{(1-f)}{V_p}K_p \quad (13)$$

where U_r is the u_r magnitude, A_p is the air bubble cross-sectional area, μ_w is the water dynamic viscosity, C_d is a user-defined drag coefficient, and R_p denotes the bubble radius controlled by the capillary number and critical Weber. The dynamic droplet size submodel, which uses the capillary values and critical Weber to compute bubble breakup, calculates the bubble sizes dynamically. The bubble breakup process in high-velocity spillway flows is dominated by shear stress and surface tension (Weber number, We). Here, the default value of 1.6 is given to the critical We, which is calculated below:

$$\mathrm{We}=\frac{\rho_m U_r^2 d_p}{8\sigma_{sur}} \quad (14)$$

where d_p is the bubble diameter and ρ_m is volume-averaged density. Furthermore, the initial bubble diameter was assumed to be 1 mm and bubble coalescence was accounted using a simple collision model (Hirt, 2016). The Richardson–Zaki coefficient multiplier and drag coefficient (explained below) were defined to default values of 0.5 and 1 for the bubble and drag force interaction, respectively. With gas escape taken into account, the minimum and maximum water volume fractions were defined as 0.1 and 1, respectively. It means that in experimental studies, an iso-surface with a 90% air concentration is used to indicate the two-phase flow surface. The air viscosity and density were defined to be 1.7×10^{-5} kg/ms and 1.225, respectively, during the spillway operation at a temperature of 15ºC. Ultimately, the critical air volume fraction, which qualifies the transition from dispersed to continuous air, was set to 1, implying that water will always be in the continuous phase, as FLOW-3D predicts. Brethour & Hirt (2009) and Hirt (2016) have more information on the drift-flux and dynamic bubble size sub-models. Larger bubbles and thus higher air fractions result from bubble coalescence, which can have a significant impact on bubble transportation and drag force. The Richardson & Zaki W. N. (1979)'s approach that improved the relative velocity to calculate the impact of relatively high air fractions was adopted by FLOW-3D. The following equation calculates improved relative velocity.

$$u_r^{eff}=u_r\times\max(0.5,f)^{k_{RZ}\,\xi_0} \quad (15)$$

where k_{RZ} is the Richardson–Zaki coefficient multiplier, which is the default value 1, and ξ_0 is the Richardson–Zaki coefficient, which is dependent on the bubble Reynolds number, $\mathrm{Re}_b=d_p u_r/\nu_w$ (where ν_w shows the water kinematic viscosity), with $\xi_0=4.45/\mathrm{Re}_b^{0.1}$ in $1<\mathrm{Re}_b\le500$, and $\xi_0=2.39$ in $\mathrm{Re}_b>500$.

Simulation Setup and Validation

To eliminate cavitation in the spillway, an aeration system including a 6-degree ramp was installed on the model of this spillway at a horizontal distance of 4.4 m from the spillway sill where the flow is almost uniform. Table (1) shows the range of variations of the parameters used to simulate the flow in this study.

For numerical flow analysis, the Flow-3D software was used. In this program, the Navier-Stokes Reynoldsian equation uses the

finite volume method to solve the mean equations, and the free surface uses the Volume of Fluid (VOF) method developed by Hirt and Nichols (1981). According to the Flow-3D model's user manual published by Flow Science Company, the RNG model is the most accurate turbulence model available for the software. Due to the dramatic effect of turbulence models on the results (turbulence is the main cause of air entrainment), the RNG model with a turbulence mixing length of 0.07 has been used. The hydraulic characteristics and concentration of air entraining the jet generated by the deflector on the Jarreh dam's spillway were measured using this software under various hydraulic operating conditions. Therefore, a 1:50 scale spillway solid view was first built using AutoCAD software. The 3D view of the AutoCAD output was then added to the Flow-3D model. In order to validate the results obtained from the Flow-3D software, the laboratory results on a physical model made in TAMAB Company were used.

Since the mesh element size is highly case-specific, a mesh sensitivity analysis was performed with three more grids to test the effect of the grid resolution on the results. The number of cells in the three examined quadrilateral grids is about 2500000 (coarse), 3300000 (medium), and 5000000 (fine), respectively. In the aerator, the minimum cell size is 1mm. The results show that a medium-sized grid is adequate for modeling the aerator flow, and that the resolution of the spillway stereolithography file is of sufficient quality. The upstream and downstream boundaries were defined as discharge and pressure boundary conditions, respectively, based on experimentally observed water depths. The side and bottom wall boundaries were used, and a symmetry boundary condition was specified at the top (zero value for normal velocity, zero gradients for the other quantities). The roughness effect was also investigated by experimenting with a variety of Manning's surface roughness coefficients that cover the range of possible values for the experimental model materials. The roughness height calculated using the Strickler formula was used to set the wall roughness. The Manning's surface roughness that resulted in the best agreement between simulated and measured discharges and flow depths was $n = 0.012\ sm^{-1/3}$. The simulations were run for a number of time steps enough to attain a statistically stationary solution and obtain converged time-averaged values. The results of the simulation of flow depth, velocity and static pressure on the spillway are shown in Fig. (3).

The results of statistical analysis are presented in Table (2). The results show that the modeling is done with good accuracy.

Table 1- Variable parameter range

Parameter	Range	Unit
Ramp angle	6, 8, 10	degree
Discharge	46.16 to 121.62	Lit/sec
Mean Depth	2.71 to 8.39	cm
Mean Velocity	2.77 to 4.81	m/sec
Static Pressure	-0.22 to 9.43	cm-H_2O

 DOI: 10.22055/JISE.2021.37743.1980

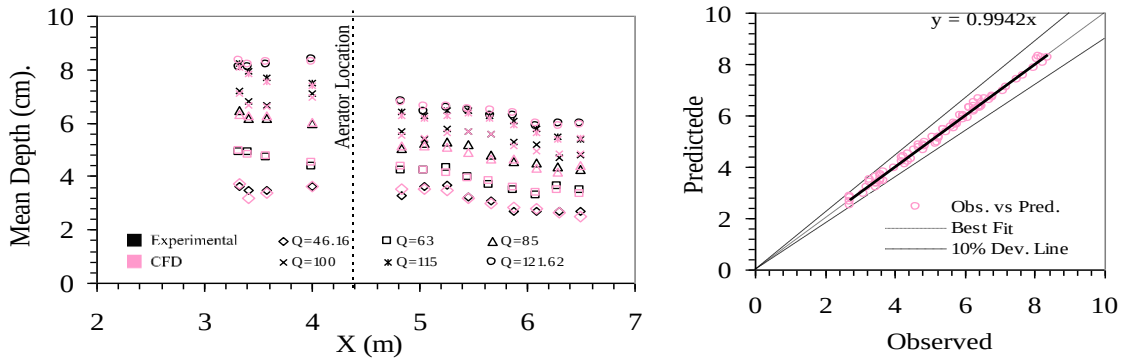

(a)

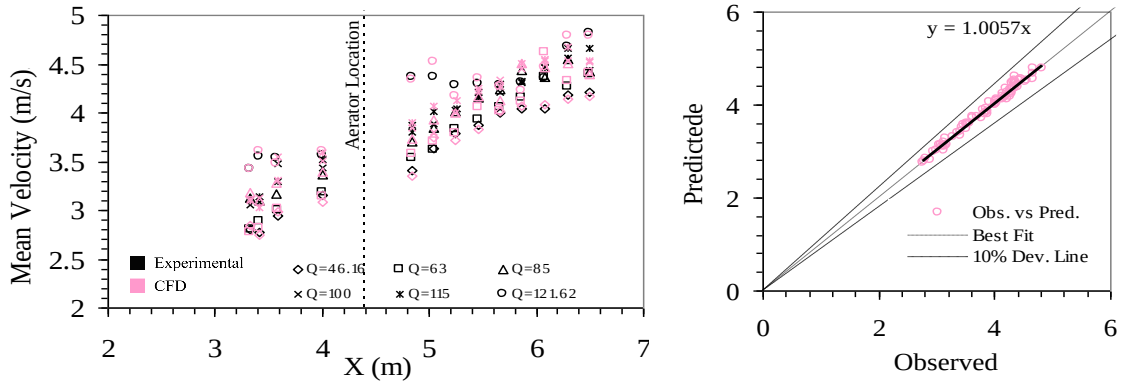

(b)

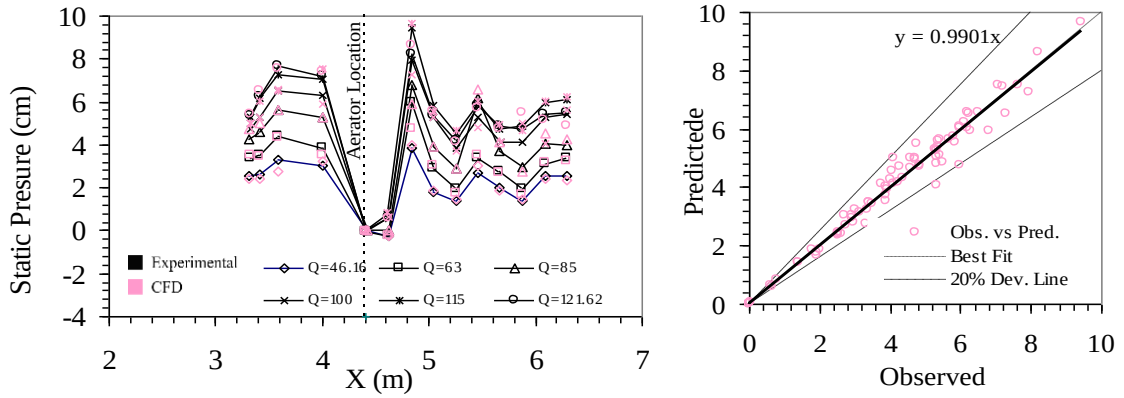

(c)

Fig. 3- Results of numerical model validation in determining a) mean flow depth, b) mean velocity, and c) static pressure in various discharges vs (Shamloo et al., 2012) research under a 6 degree ramp angle

Table 2- Statistical Error Function

Parameter	Root Mean Square Error	Main Absolute Error	Standard Error of Estimate	Deviation Coefficient
Mean Depth (cm)	0.1345	0.1193	0.1324	0.9942
Mean Velocity (m/sec)	0.0768	0.0625	0.0742	1.0057
Static Pressure (cm)	0.3462	0.2273	0.347	0.9901

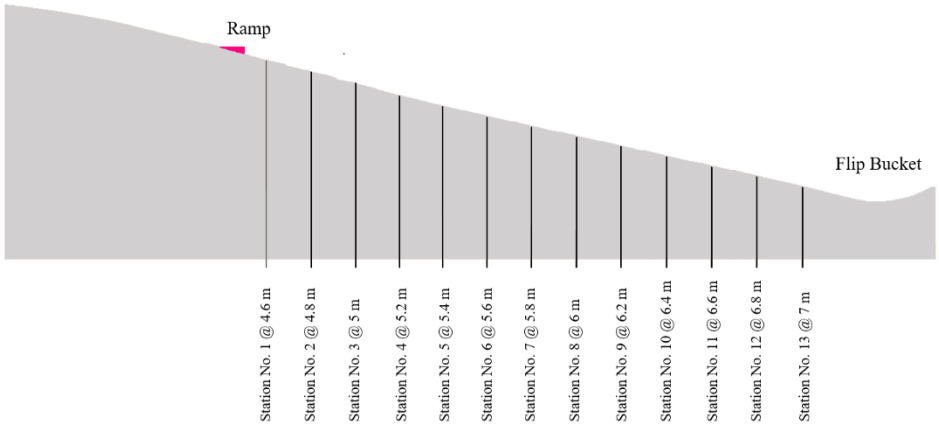

Fig. 4- Location of data extraction stations after aeration on a scale model of 1:50

After ensuring the accuracy of the model results by changing the ramp angle, the amount of air entering the flow as well as the percentage of aeration, and changes in the cavitation index during the spillway were evaluated under different scenarios of ramp slope. For this purpose, in addition to the ramp angle of 6 degrees, a ramp model with slopes of 8 and 10 degrees was prepared. During the chute after aeration, 13 measuring stations were determined at a distance of 20 cm from each other and changes in static pressure and cavitation index in the direction of the chute were determined for different discharges in the middle of the spillway. Fig. (4) shows the position of the measuring stations.

Results

In this research, the value of air entraining the flow through the aerator is measured at the downstream of aerator with three ramp angles of 6, 8, and 10 degrees for flow discharge from 46.16 to 121.62 liters per second (before the collision region). The theory behind air entrainment into liquid surfaces is that turbulent flows form small liquid elements above water free surface that can capture air and move it to the liquid body. The extent to which liquid elements can rise above the free surface of water depends on whether the intensity of the turbulence is sufficient to overcome the surface gravity and surface tension. The air entraining the flow and the aeration ratio are calculated using equations (16) and (17).

$$Q_{air} = \bar{C} \times V \times A \qquad (16)$$

$$\beta = Q_{air} / Q_w \qquad (17)$$

where Q_{air} is the entreating air discharge, A the cross section of the flow in square meters, V the mean flow velocity in meters per second, $\overline{C}$ the average air concentration, and β aeration ratio.

The value of air entraining the flow with ramp angles of 6, 8 and 10 degrees was also measured in order to achieve the main objective of this study. The effect of ramp angle on the value of air entraining the flow jet for all the discharges is shown in Fig. (5). The results show that as the flow discharge increases, flow velocity and turbulence increase, increasing the air flow absorption into the flow through the deflector. The value of turbulence increases as the deflector angle increases, as does the value of air entraining the free jet. The length of the jet nappe is shortened as the flow discharge increases due to the increased weight of the jet nappe and its early contact with the chute floor. The smaller the deflector angle, the sooner this will be achieved. The contact surface of the bottom of the jet with the air inside the duct decreases as the length of the jet nappe is shortened, resulting in less air entering the jet. This has also been achieved at the ramp angles of 8 and 10 degrees, but has not been reported since the flow conditions on the structure were not considered for potentials greater than the design potential. Note that the laboratory results of Shamloo et al. (2012) also confirmed this.

Fig. (6) shows the variations in aeration coefficient in relation to the spillway flow

 DOI: 10.22055/JISE.2021.37743.1980

discharge β for all the three angles. According to the figure, the value of β decreases as the flow discharge increases.

This is due to the increase in flow volume, which shortens the jump length of the jet, and in cases where the water jet hits the spillway surface, part of it is directed upstream of the collision, leading to inadequate aeration of the water jet. The aeration coefficient increased first and then decreased for the ramp angle of 6 degrees, as shown in the figure, indicating that aeration had the least effect at a flow rate of 46.16 liters per second. The maximum effect of aeration is also at an angle of 10 degrees and in discharge of 46.16 liters per second. It should be noted that the results of this study are valid over a wide range of parameter changes.

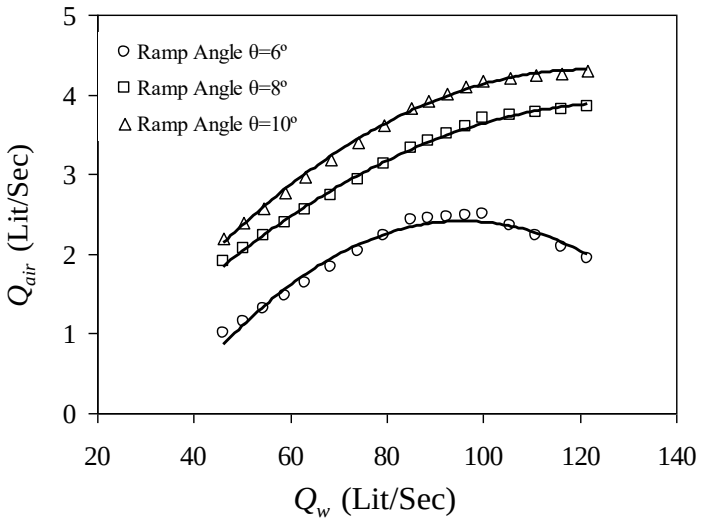

Fig. 5-The effect of ramp angle on the value of air entraining the flow jet

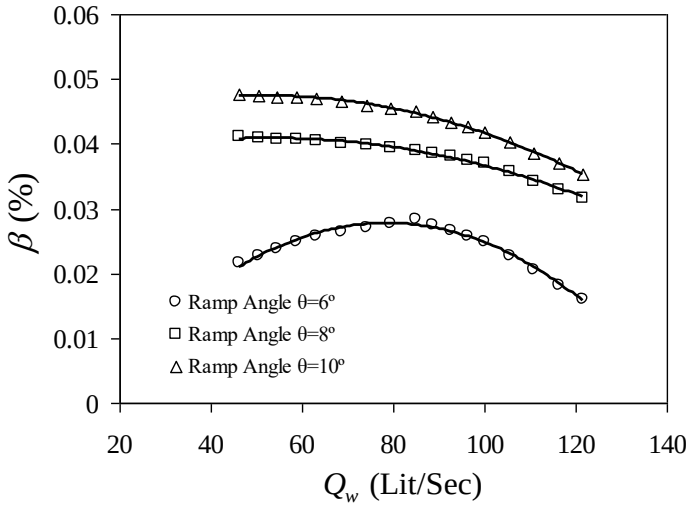

Fig. 6- The effect of ramp angle on the value of air entraining the flow jet

In order to calculate the cavitation index in the stations shown in Fig. (4), the following relation can be written:

$$\sigma = \frac{P - P_v}{\rho \alpha V_o^2 / 2g} \quad (18)$$

where P is the absolute pressure, P_v water vapor pressure and V_o is the mean flow velocity.

Eq. (18) can be rewritten as Eq. (19) in the flow with free surface in spillways by considering the vertical arc in the floor:

$$\sigma = \frac{P_{atm}/\gamma - P_v/\gamma + h\cos\theta + h/g\left(V_o^2/r\right)}{\alpha V_o^2/2g} \quad (19)$$

In this model, P_{atm}/γ or the atmospheric ambient pressure is assumed to be 1atm or 10.33 meters of water. The parameter P_v/γ is the amount of water vapor pressure, which at a temperature of about 25°C is equal to 0.33 m of water height.

In calculations to consider the appropriate safety factor, this value is assumed to be equal to 1 meter of water height. Parameter $h\cos\theta$ or P_o/γ shows the amount of pressure (pressure such as water height) that is on the structure in different parts. The parameter $\alpha V_o^2/2g$ is energy line height (in meters) in the desired section. Besides, parameter $h/g \times \left(V_o^2/r\right)$ shows the pressure difference due to the presence of vertical arcs. Substituting the above values into Eq. (19) we have:

$$\sigma = \frac{(10.33 - 1 + P_o/\gamma)}{\alpha V_o^2/2g} = \frac{2g}{\alpha V_o^2}\left(9.33 + \frac{P_o}{\gamma}\right) \quad (20)$$

Using the values of pressure and velocity calculated by the model in each of the sections and by substituting in Eq. 20, the values of cavitation coefficient in each section were calculated. The results are presented in Fig. (7). In this model, the critical value of the cavitation index, considering the reliability coefficient, is 0.2.

As is known, by moving away from the spillway sill due to the increase in velocity and decrease in pressure, the values of the cavitation coefficient decrease in all flows. In this model, for a discharge of 121.62 lit/sec, the minimum amount of cavitation index is calculated to be 0.24, which is related to cross-sections 12 and 13 placed at a distance of 6.8 and 7 meters, respectively, from the spillway sill. Considering that with increasing the ramp angle, the amount of pressure in the measured sections increases, it is expected that the cavitation index also increases with increasing the ramp angle, which is clearly seen in Fig. (7). The analysis of the results shows the superior performance of aerator when deflector angle is ten degrees. Statistical analysis of the results shows that the aeration system with a ramp angle of 10 degrees shows the average values of cavitation index between 9 to 13 percent higher than the estimated values under the ramp angle of 8 degrees. Moreover, the values of cavitation index obtained under the ramp angle of 8 degrees are on average between 5 to 9.8% higher than the values with the ramp angle of 6 degrees. Note that the cavitation index is calculated based on the average flow velocity in Equation (20) instead of the flow velocity near the floor, which is a matter of confidence. In addition, velocity changes versus the increase of ramp angle in measurement sections were very small and had little effect on the impact of static pressure changes on the cavitation index in terms of the increase of ramp angle. In other words, the increase of pressure due to the increase of ramp angle had a greater effect on cavitation index values.

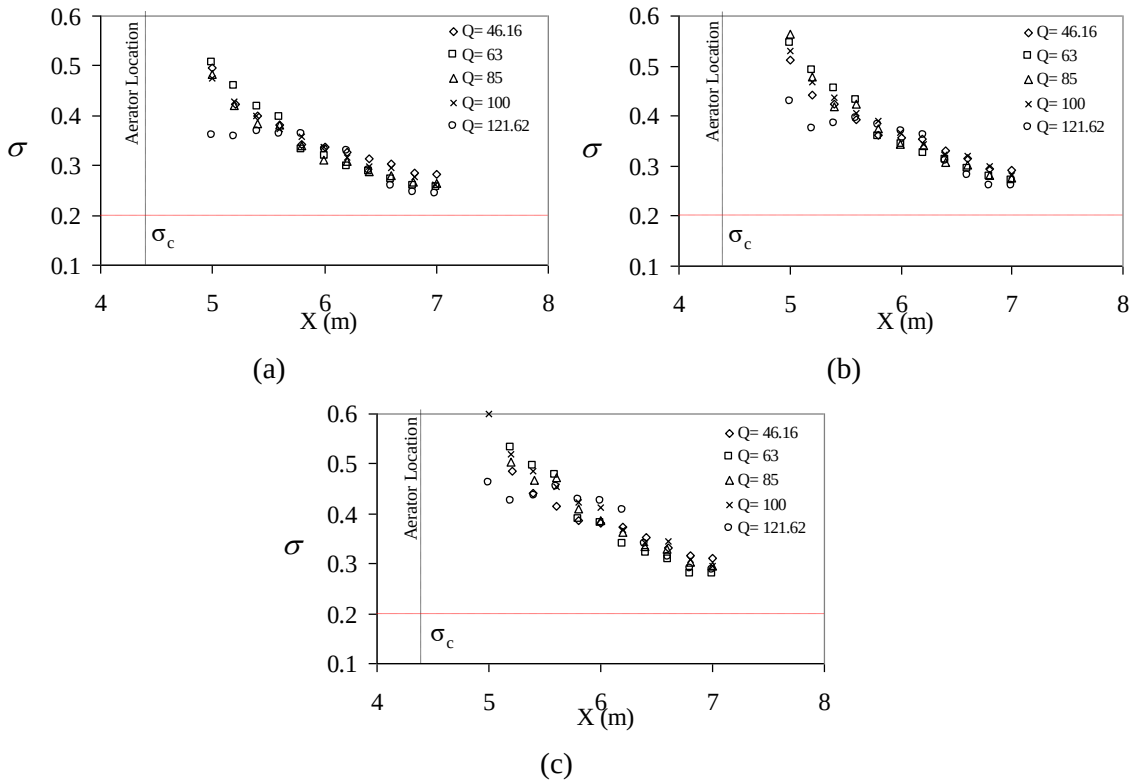

Fig.7- Changes in cavitation index in different discharges with changes in ramp angle: a) 6 degrees, b) 8 degrees and c) 10 degrees

Conclusion

A nappe entrainment through the upper and lower free surfaces of the jet, an extra quantity of air entrained by plunging jet entrainment, and a recirculation process within the cavity define air entrainment above an aerator. The computation of the jet trajectory and the location of the impact point are two important aspects of air entrainment. As a result, the jet angle relative to the spillway floor at the impact point is important in this research. Using the Flow-3D model, the efficiency of aeration and the effect of ramp angle on aeration discharge in the Jarreh spillway were simulated under various hydraulic flow conditions.

The results show that as the ramp angle increases, the value of turbulence increases, and hence the air entraining the flow jet increases. By increasing the ramp angle, the amount of pressure in the measured sections, the turbulence in the pressure distribution in the chute, and thus the cavitation index value increase. The analysis of the results indicates the relative superiority of aeration efficiency at a ramp angle of ten degrees. Overall, the results show that the Flow-3D software is able to simulate two-phase flows on spillways.

.

Acknowledgment

The authors would like to thank the Jundi-Shapur University of Technology for their supports

References

1- Baharvand, S., & Lashkar-Ara, B. (2021). Hydraulic design criteria of the modified meander C-type fishway using the combined experimental and CFD models. *Ecological Engineering*, *164*. https://doi.org/10.1016/j.ecoleng.2021.106207

2- Bayon, A., Toro, J. P., Bombardelli, F. A., Matos, J., & López-Jiménez, P. A. (2018). Influence of VOF technique, turbulence model and discretization scheme on the numerical simulation of the non-aerated, skimming flow in stepped spillways. *Journal of Hydro-Environment Research*, *19*, 137–149.

https://doi.org/10.1016/j.jher.2017.10.002

3- Brethour, J. M., & Hirt, C. W. (2009). Drift Model for Two-Component Flows. *Flow Science, Inc., FSI-09-TN83Rev*, 1–7.

4- Chanson, H. (1989). Study of air entrainment and aeration devices. *Journal of Hydraulic Research*, *27*(3), 301–319. https://doi.org/10.1080/00221688909499166

5- Dong, Z., Wang, J., Vetsch, D. F., Boes, R. M., & Tan, G. (2019). Numerical simulation of air-water two-phase flow on stepped spillways behind X-shaped flaring gate piers under very high unit discharge. *Water (Switzerland)*, *11*(10). https://doi.org/10.3390/w11101956

6- Flow-3D, V. 11. 2. (2017). User Manual. *Flow Science Inc.: Santa Fe, NM, USA;*

7- Hirt, C. W. (2003). Modeling Turbulent Entrainment of Air at a Free Surface. *Flow Science, Inc.*, *FSI-03-TN6*, 1–9.

8- Hirt, C. W. (2016). Dynamic Droplet Sizes for Drift Fluxes. *Flow Science, Inc.*, 1–10.

9- Hirt, C. W., & Nichols, B. D. (1981). Volume of fluid (VOF) method for the dynamics of free boundaries. *Journal of Computational Physics*, *39*(1), 201–225. https://doi.org/10.1016/0021-9991(81)90145-5

10- Kherbache, K., Chesneau, X., Zeghmati, B., Abide, S., & Benmamar, S. (2017). The effects of step inclination and air injection on the water flow in a stepped spillway: A numerical study. *Journal of Hydrodynamics*, *29*(2), 322–331. https://doi.org/10.1016/S1001-6058(16)60742-4

11- Kramer, M., & Chanson, H. (2019). Optical flow estimations in aerated spillway flows: Filtering and discussion on sampling parameters. *Experimental Thermal and Fluid Science*, *103*, 318–328. https://doi.org/10.1016/j.expthermflusci.2018.12.002

12- Mahmoudian, Z., Baharvand, S., & Lashkarara, B. (2019). Investigating the Flow Pattern in Baffle Fishway Denil Type. *Irrigation Sciences and Engineering (JISE)*, *42*(3), 179–196.

13- Meireles, I. C., Bombardelli, F. A., & Matos, J. (2014). Air entrainment onset in skimming flows on steep stepped spillways: An analysis. *Journal of Hydraulic Research*, *52*(3). https://doi.org/10.1080/00221686.2013.878401

14- Parsaie, A., & Haghiabi, A. H. (2019). Inception point of flow aeration on quarter-circular crested stepped spillway. *Flow Measurement and Instrumentation*, *69*. https://doi.org/10.1016/j.flowmeasinst.2019.101618

15- Richardson, J. F., & Zaki W N. (1979). Sedimentation and Fluidisation. Part 1. *Trans. Inst. Chem. Eng*, *32*, 35–53.

16- Shamloo, H., Hoseini Ghafari, S., & Kavianpour, M. (2012). Experimental study on the effects of inlet flows on aeration in chute spillway (Case study: Jare Dam, Iran). *10th International Congress on Advances in Civil Engineering, Middle East Technical University, Ankara, Turkey*.

17- Wang, S. Y., Hou, D. M., & Wang, C. H. (2012). Aerator of stepped chute in Murum Hydropower Station. *Procedia Engineering*, *28*, 803–807. https://doi.org/10.1016/j.proeng.2012.01.813.

18- Wei, W., Deng, J., & Zhang, F. (2016). Development of self-aeration process for supercritical chute flows. *International Journal of Multiphase Flow*, *79*, 172–180. https://doi.org/10.1016/j.ijmultiphaseflow.2015.11.003

19- Wu, J., QIAN, S., & MA, F. (2016). A new design of ski-jump-step spillway. *Journal of Hydrodynamics*, *05*, 914–917.

20- Xu, Y., Wang, W., Yong, H., & Zhao, W. (2012). Investigation on the cavity backwater of the jet flow

from the chute aerators. *Procedia Engineering*, *31*, 51–56. https://doi.org/10.1016/j.proeng.2012.01.989

21- Yakhot, V., & Orszag, S. A. (1986). Renormalization group analysis of turbulence. I. Basic theory. *Journal of Scientific Computing*, *1*(1), 3–51. https://doi.org/10.1007/BF01061452

22- Yang, J., Teng, P., & Lin, C. (2019). Air-vent layouts and water-air flow behaviors of a wide spillway aerator. *Theoretical and Applied Mechanics Letters*, *9*(2), 130–143. https://doi.org/10.1016/j.taml.2019.02.009

23- Zhang, G., & Chanson, H. (2016). Interaction between free-surface aeration and total pressure on a stepped chute. *Experimental Thermal and Fluid Science*, *74*, 368–381. https://doi.org/10.1016/j.expthermflusci.2015.12.011

© 2021 Shahid Chamran Universiry of Ahvaz, Ahvaz, Iran. This article is an open access article distributed under the terms and conditions of the Creative Commons Attribution 4.0 International (CC BY 4.0 license) (http://creativecommons.org/licenses/by/4.0/).